arXiv:1808.05307v2 [physics.data-an] 28 Aug 2018

Treatment of material radioassay measurements in projecting sensitivity for low-background experiments

R.H.M. Tsang[a,*], I.J. Arnquist[a], E.W. Hoppe[a], J.L. Orrell[a], R. Saldanha[a]

[a]*Pacific Northwest National Laboratory, Richland, WA, USA*

Abstract

By analyzing sensitivity projections as a statisical estimation problem, we evaluated different ways of treating radioassay measurement results (values and upper limits) when projecting sensitivity for low-background experiments. We developed a figure of merit that incorporates a notion of conservativeness to quantitatively explore the consequences of attempts to bias sensitivity projections, and proposed a method to report sensitivity.

Keywords: low background experiments, material assay measurements, upper limits and uncertainty

PACS: 95.35.+d, 23.40.-s, 29.40.-n, 02.50.-r, 06.20.Dk

2010 MSC: 62K99, 62P35, 65G99, 65Z05

1. Introduction

Modern low-background experiments in dark matter and neutrinoless double beta decay research rely on material assay measurements of trace level radioactive impurity concentrations to model and project their anticipated experimental sensitivity.

*Corresponding author, heiman.tsang@pnnl.gov

Experimental collaborations have reported detailed records of their material assay measurement programs (e.g., [1, 2, 3, 4, 5, 6, 7, 8]) in preparation for construction of their experiments. A research community online database [9] has collected these and other measurements to provide a resource for searching and identifying material assay measurements across multiple low background experiments for a wide variety of materials. Researchers use these references to estimate potential levels of trace radioactivity that may be present in experimental conceptualizations.

In the ideal scenario, experimental sensitivity projections would use reported material assay measurement *values* well above the methodological detection limit of the assay measurement apparatus, with respect to their quantified *uncertainties*. However, in many cases experimental collaborations are finding and selecting ultra-pure materials that can only be quantified as having a radioimpurity concentration level given as an *upper limit*, dependent upon the material assay methodological detection limit. As a result, next generation low-background experiments in dark matter and neutrinoless double beta decay research produce sensitivity projections using a mixture of material assay measurement *values* and *upper limits*.

Some researchers choose to be "conservative" and set the upper limit as a *value* while others choose to transform the upper limit to a distribution, either uniform or some variations of the Gaussian distribution, effectively treating the radioimpurity concentration like a Bayesian prior. This adds some Bayesian elements into an otherwise completely frequentist procedure. Naturally one expects these different choices to result in different predictions of experimental performance. To our knowledge, the impact of these choices

has not been studied in a systematic fashion.

In the following sections, we describe our study on the impact of these choices. We begin by illustrating the problem using a simple example in Section 2. Then, in Section 3, we briefly review two common assay techniques and discuss their similarities and differences. Next, in Section 4, we describe a Monte Carlo model of a typical assay campaign from material selection to sensitivity projection, and the different ways to treat assay values and upper limits. The results of the Monte Carlo model are shown in Section 5. In Section 6, we define a figure of merit to evaluate those choices, apply it to various scenarios, and propose a method to report sensitivity. Finally, we summarize in Section 7.

2. Combining a measurement with an upper limit

To begin with a very simplified example, consider a small experimental arrangement composed of two materials, A and B. Material A was evaluated through a material assay method and was determined to contain a concentration of radioimpurity X at a level of 11.1 ± 1.2 μBq/kg. Material B was evaluated in the same fashion and was determined to contain a concentration of radioimpurity X at a level of *less than* 0.8 μBq/kg, depending on the technology used and the institution reporting the limit.

From a high statistics radiation transport simulation, it is determined that materials A and B will contribute to the background event rate of the small experimental arrangement with approximately a ratio of 1:10.2,. This implies that both materials will contribute to the total background rate at roughly equivalent rates, if one presumes the actual *true* radioimpurity

level of material B is at or just below the instrument sensitivity. Table 1 captures the key inputs for projecting the background event rate in this small experimental arrangement.

Material	Mass	Radio-impurity X	Simulation information		
	[kg]	[μBq/kg]	Primaries	Background Events	Efficiency, ε [Hz/Bq]
A	10	11.1 ± 1.2	10^8	100,234	0.00100
B	10	< 0.8	10^8	1,022,387	0.01022

Table 1: Information from material assay measurements and high statistics radiation transport simulation for a small experimental arrangement composed of two materials, A and B. This simplified experimental example is entirely hypothetical, deliberately constructed to elucidate the issue under study in this paper.

The question arises: how to quantitatively combine the radioimpurity concentration of X in materials A and B in projecting the expected experimental background rate in this small experimental arrangement? It is clear that, if we only consider material A, we should expect a background event rate, R_A, contribution of approximately 1.1×10^{-7} Hz, or about 3.5 ± 0.4 background events for an uninterrupted year of data collection. These values, respectively, are determined using the following two equations:

$$R_i = \varepsilon_i \cdot M_i \cdot X_i \tag{1}$$

$$C_i = R_i \cdot \tau \tag{2}$$

where i refers to material A or B; The variables ε_i, M_i, and X_i, are the hit efficiency, the mass, and the radioimpurity concentration, of material i, with example values given in Table 1. The quantity τ is the livetime of the experiment and C_i is the number of background events expected in the experiment due to material i.

If we assume the worst case (or "most conservative" assumption) regarding the background event rate contribution from material B, we employ the same two equations (1) and (2) and insert the *upper limit* into the calculation. Doing so suggests a background event rate contribution of approximately 0.8×10^{-7} Hz, or about 2.6 background events for an uninterrupted year of data collection. Note it is now not clear how to represent the uncertainty on the number of background events in a year of data collection since we do not know the uncertainty associated with the underlying measurement of the radioimpurity concentration of X in material B.

To devise a way to treat an upper limit, we first need to understand why an upper limit is reported and how it is calculated, and this depends on the assay technique used. (For ease of discussion, all upper limits are at 90% C.L. unless stated otherwise.)

3. Assay methodologies

Many material assay techniques are employed by collaborations developing low background experiments as a means to measure ultra-trace levels of radioimpurities in materials as an evaluation of feasibility in advance of proposal or construction. Two common techniques are,

- Radiometric counting with high purity germanium (HPGe) gamma-ray

spectrometers, and

- Ion counting with inductively coupled plasma mass spectrometry (ICP-MS).

3.1. High purity germanium assay (HPGe)

The concentrations of radioimpurities in a material sample can be measured by gamma ray spectrometry with HPGe detectors through identification of the characteristic gamma-rays emitted from the decays of isotopes present in the material.

In a typical setup, a LN_2-cooled HPGe detector is housed in a chamber shielded from the ambient radiation by copper and lead. The sample to be assayed, usually 10 to 10^3 g in mass, is placed in the same chamber. Gamma rays emitted by the radioimpurities in the sample deposit energy in the Ge crystal.

Background sources in the HPGe instrument include ambient radiation, cosmic ray induced energy deposits or activation, and internal radioimpurities in the detector. With sufficient shielding, ambient radiation is usually not a major source of background and the effect of direct cosmic ray interactions can be reduced by using a muon veto or locating the detector underground. However, the effects of long-lived cosmogenic isotopes and internal radioimpurities cannot be easily removed. This remaining background is measured through weeks-long background runs taken every several months.

Some of the gamma rays will deposit all of their energy in the Ge crystal, contributing to the so-called full peak. The area of the full peak provides an estimate of the specific activity of the radioimpurity in question. More

precisely,

$$X = \frac{1}{D} \cdot (s - b) \tag{3}$$

where X is the specific activity of radioimpurity [Bq/kg]; s and b are the areas under the gamma ray spectra near the full peak in the sample run and the background run respectively [cps]; D is the detection sensitivity [cps/(Bq/kg)] (aka efficiency), which equals $m \cdot f \cdot \epsilon(E)$ where m is the mass of the sample [kg]; f is the branching fraction of the gamma ray; and $\epsilon(E)$ is the hit efficiency to be calibrated by detector simulation and/or radiation sources of known activity such as NIST traceable standards. The error associated with $\epsilon(E)$ will not be considered in this study.

For this study whether to report a measured value or an upper limit is decided by the Feldman-Cousins (FC) approach [10] at a certain C.L., e.g. 90%. We choose to use the FC method in this study because it is a readily reproducible prescriptive method available in the literature. The reporting heuristic is: if the lower limit evaluated by the FC approach equals zero, then an upper limit is reported in the form of "$X < U_X$ at 90% C.L.", where

$$U_X = \frac{1}{D \cdot t} \mathrm{FC}_{\mathrm{UL}}^{90\%} (s \cdot t,\ b \cdot t) \tag{4}$$

and $\mathrm{FC}_{\mathrm{UL}}^{90\%}$ is the upper limit evaluated by the FC approach at 90% C.L., and t is the HPGe run time. Otherwise, a measurement value is reported in the form of "$X \pm \sigma_X$" where $\sigma_X = \frac{1}{D}\sqrt{\frac{s+b}{t}}$,

3.2. Inductively coupled plasma mass spectrometry (ICP-MS)

While there are a variety of techniques for introducing samples to an ICP-MS, the vast majority of analyses introduce samples to the instrument in the form of a dissolved aqueous solution. The solution is nebulized into a fine aerosol in an argon carrier gas before introduction into the high temperature plasma (*ca.* 6000-8000 K) where the dissolved components are atomized and ionized. The ions are directed through some ion optics in a high vacuum chamber before being mass resolved based on the mass-to-charge ratio of the ion in the mass analyzer and detected.

ICP-MS analyses use "process blanks" to account for the background contribution from the sample preparation steps prior to analysis (e.g., acid digestions, dilutions, purity from added reagents, etc.). The process blanks allow the sensitivity reach (detection limits) for the analysis to be determined. In these ways ICP-MS has effectively the same underlying metrological and methodological requirements of HPGe counter, though they are implemented through differing means.

The sample and blank measurements are collected in units of counts per second. The count rates can be converted to impurity concentration as follows,

$$X = \frac{s}{D_s} - \frac{1}{n}\sum_{i}^{n}\frac{b_i}{D_{b_i}} \tag{5}$$

where s is the count rate for the analyte in the sample [cps]; b_i is the count rate for the analyte in the ith blank [cps] out of a total of n blanks; D_s and D_{b_i} are the detection sensitivities [cps/ppt].

The detection sensitivities can be determined using a number of methods,

but at PNNL, where we use isotope dilution methods, we determine the sensitivities using added non-naturally occurring tracers,

$$D_s = \frac{s'}{X'} \tag{6}$$

$$D_{b_i} = \frac{b'_i}{X'} \tag{7}$$

where the primed values are associated with the tracer. Here, for simplicity, we assume all the samples and blanks are spiked with the same amount of tracer.

Substituting equations 6 and 7, equation 5 becomes,

$$X = X' \cdot \left(\frac{s}{s'} - \frac{1}{n} \sum_{i}^{n} \frac{b_i}{b'_i} \right) \tag{8}$$

Despite the similarity to HPGe in terms of its counting statistics nature, the convention for reporting measurement results is somewhat different. As an example, for ICP-MS measurements made at PNNL, the convention is: if $s < 3\sigma_b$, where σ_b is the standard deviation of the ratios $\frac{b_i}{b'_i}$, then $3\sigma_b$ would be reported as the detection limit (approximately 95% C.L. based on Student's t with 2 degrees of freedom); otherwise, report $X \pm \sigma_X$ as the measurement result where

$$\sigma_X = X' \cdot \sqrt{\left(\frac{s}{s'}\right)^2 \left[\left(\frac{\sigma_s}{s}\right)^2 + \left(\frac{\sigma_{s'}}{s'}\right)^2 \right] + \sigma_b^2} \tag{9}$$

and σ_s and $\sigma_{s'}$ are the errors on s and s' respectively.

3.3. Summary of assay methodologies

One basic difference between ICP-MS and HPGe counting is how variability is introduced by sample preparation. Because the sample is typically introduced to the instrument in the form of a solution, ICP-MS relies upon significantly more sample preparation steps than HPGe, typically requiring more added reagents and sample digestion steps. However, ICP-MS measurements are buttressed with process blank preparations and measurements along with the most accurate and precise quantitation method for ICP-MS by employing isotope dilution [11, 12]. HPGe counting minimizes sample preparation, but at the cost of assumptions made regarding the background stability of the counting apparatus and the appropriateness of calibration standards to be representative of the sample being measured. The concern for variability in either case, ICP-MS or HPGe, is whether the statistical distribution for repeated measurements obeys Poisson statistics. This can be tested, via good laboratory practice, in both cases. For the purposes of this study, we presume such good laboratory practice is achieved as the goal of this study is to understand how the different treatments of assay results impact sensitivity projections rather than to evaluate the assay methodologies.

Another point to note is that the two methods typically have very different detection sensitivities. ICP-MS can reach sub-ppt detection (μBq/kg) levels with tens of milligrams of sample material. In comparison, HPGe is typically 2-3 orders of magnitude less sensitive than ICP-MS, even though hundreds of grams of sample material is typically used. However, the magnitude of detection sensitivity has no direct effect on the statistical distribution of repeated measurements.

Time variation in detection sensitivity D is known to exist in both HPGe [13] and ICP-MS [14]. For HPGe, detection sensitivity D is periodically calibrated with button sources; while for ICP-MS, *in situ* tracers are used to estimate D for every run. These methods establish an *average* D for a run. Therefore the treatment of time variation in both methods are mathematically identical.

Another difference is that HPGe and ICP-MS count different species. HPGe counts the gamma rays from the radioactive decays of the impurity and/or its progenies, while ICP-MS counts the ions of the parent isotope of the decay chain. The results from the two techniques can be compared when the impurity in the sample is in secular equilibrium. In other words, under this assumption, the measurement results of HPGe and ICP-MS can be seen as the same quantity merely in different units (Bq/kg vs ppt), as can their detection sensitivities D (cps/(Bq/kg) vs cps/ppt).

To sum up, despite the apparent differences discussed above, with good laboratory practice and the assumption of secular equilibrium, whether a measurement is made by HPGe counting or ICP-MS has no effect on its statistical properties relevant to this study.

4. Model of assay, experiment, and sensitivity

4.1. Hypothetical experiment

Dark matter and neutrinoless double beta decay experiments ($0\nu\beta\beta$) are the primary large, low-background experiments facing the issue of treating *upper limits* in their material assay results when modeling their experimental sensitivity. We choose to focus on a simplified model of a hypothetical $0\nu\beta\beta$

decay experiment to further explore the impact of treating material assay *upper limits*. This choice benefits from the signature of the $0\nu\beta\beta$ decay: A search for an energy peak (typically Gaussian) at the known Q-value, $Q_{\beta\beta}$, of the decay. For this reason our hypothetical experiment can largely be treated as a counting experiment, closely aligned with the earlier discussions within this paper regarding counting statistics. This is in contrast to employing a hypothetical model of a dark matter experiment, where we would need to bring in details of the dark matter hypothesis that are unrelated to the focus of this paper.

Detector. Our hypothetical $0\nu\beta\beta$ detector consists of N parts with masses M_i, impurity concentrations X_i and hit efficiencies ε_i. The fiducial volume contains one metric ton of radiopure ^{136}Xe.[1] The impurity concentrations X_i are assumed to be uncorrelated. The livetime of this hypothetical experiment is assumed to be 10 years.

As seen in Equation 1, since M_i and ε_i always appear as a product, for the purpose of sensitivity projection, we can assume $M_i = 1$ for all i without loss of generality, as the variation in mass can be absorbed into ε_i. Therefore, the detector can be completely specified by two one-dimensional arrays, $\{X_i\}$ and $\{\varepsilon_i\}$ (with N implicitly specified by the size of the arrays).

Assay. Given the discussion of Section 3 and a desire for simplicity we assume that all materials are assayed with an HPGe detector. We further assume that, in the materials, there is only one relevant radioimpurity whose

[1] A specific isotope, here ^{136}Xe, is chosen just for concreteness. This study does not depend on the isotope choice.

concentration is estimated by integrating the HPGe measured counts in a narrow region of interest around the spectral peak at the characteristic energy of the one gamma-ray that it emits. For ease and no loss of generality towards our purpose, the detection efficiency for the radioisotope is assumed to be 100%. The HPGe detector is assumed to have a background rate of 10 cpd in the region of interest. All material samples used for assay are one kg, and are counted for 14 days. The background runs are also 14 days long and each background run is paired with only one sample run.

An assay measurement by the HPGe detector is simulated by drawing two Poisson random variables, representing the sample counts and the background counts. Results are analyzed and reported following the heuristic described above in Section 3.1. The central values (negative or not) and their uncertainties are always reported, so that they can potentially be used in defining a prior.

Under these assumptions, the detection sensitivity D is 10^{-6} cps/(μBq/kg), and the background rate b is 10 cpd (or 1.16×10^{-4} cps). It can be shown that a sample with impurity concentration of $X = 23.8$ μBq/kg would be barely detectable by this detector. (See Appendix A for derivation.)

4.2. Sensitivity method

In a nutshell, the projected sensitivity is calculated by a Monte Carlo method [2], in which a large number of toy experiments are simulated under the null hypothesis. Each toy represents a possible realization of the experiment, where an upper limit on the signal can be set. The mean of these upper limits is the rate sensitivity which can be converted to a half-life sensitivity. (See Appendix B for discussion.) The calculation procedures are detailed

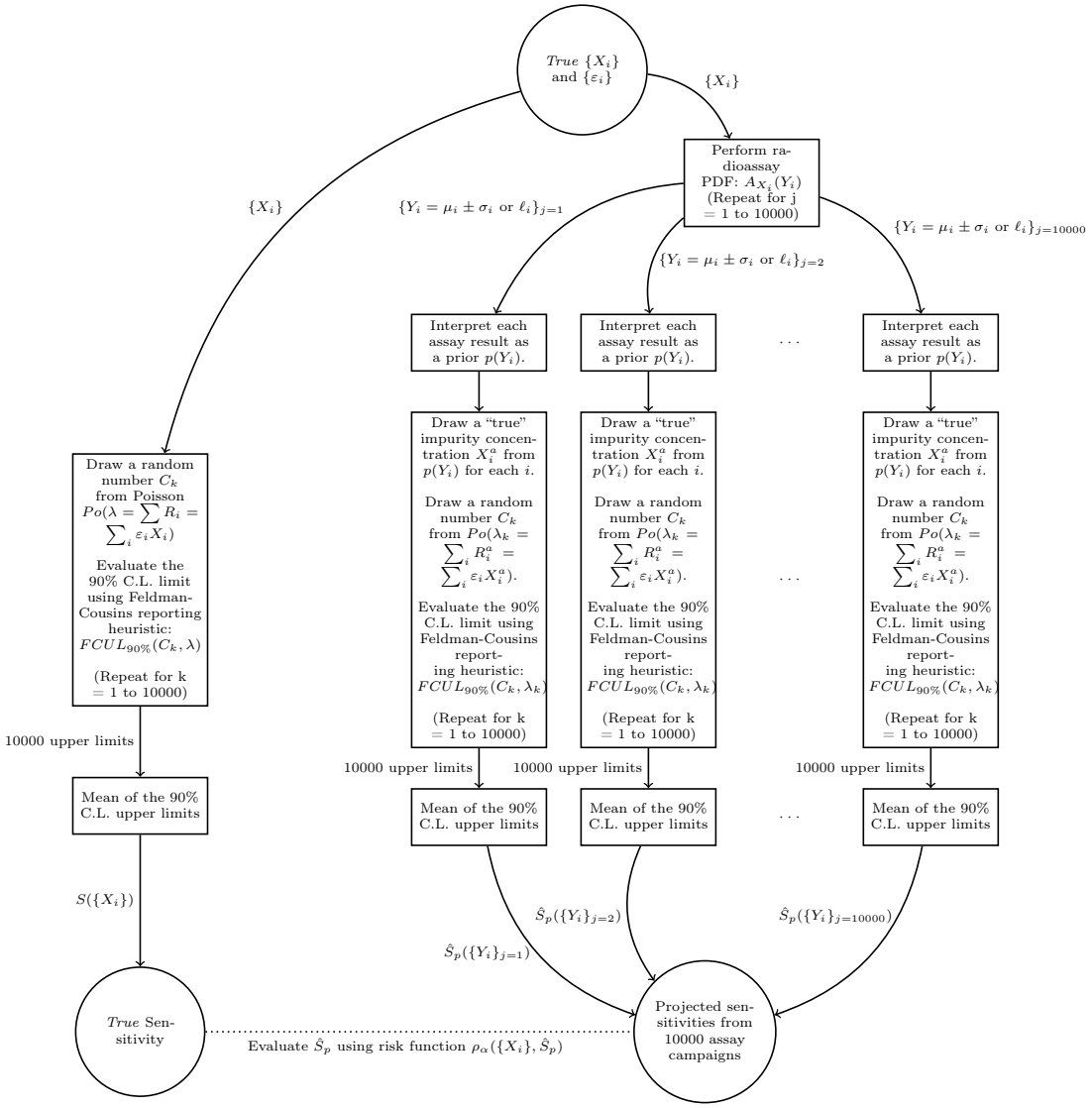


Figure 1: Diagram of the implementation of the sensitivity calculation. Here $\{X_i\}$ is the set of the *true* impurity levels for all the detector parts (of index i.) Likewise $\{Y_i\}$ is a set of the impurity levels for all detector parts *derived* from a model of the radioassay measurement process. The index, j, represents the imagining performing all radiopurity assays multiple times, with each case representing one possible way the radioassay program might report derived impurity levels $\{Y_i\}$ based on the *true* impurity levels $\{X_i\}$.

below, also illustrated in Figure 1.

4.2.1. Sensitivity based on perfect knowledge

If the actual *true* impurity concentrations of the detector parts are known (as we can in our idealized model), the expected background count (λ) can be calculated precisely as $\lambda = \sum_i R_i = \sum_i \varepsilon_i X_i$, and the background counts realized in the toys (C_k) are drawn from the Poisson distribution, $Po(\lambda)$. The following procedure is repeated 10000 times (numbering, k) to produce an ensemble of possible outcomes for the toys:

1. Draw a random number from $Po(\lambda)$, and assign it to C_k.
2. Calculate the 90% C.L. upper limit for an experiment with expected background count λ and measured count C_k using the FC reporting heuristic.
3. Append the upper limit to an array used to collect the ensemble of outcomes for the toys.

In this case, as we have perfect knowledge of the impurity levels in this hypothetical study, the *true* half-life sensitivity (S) is calculated as

$$S = N_{Xe} \ln(2)/S_R \tag{10}$$

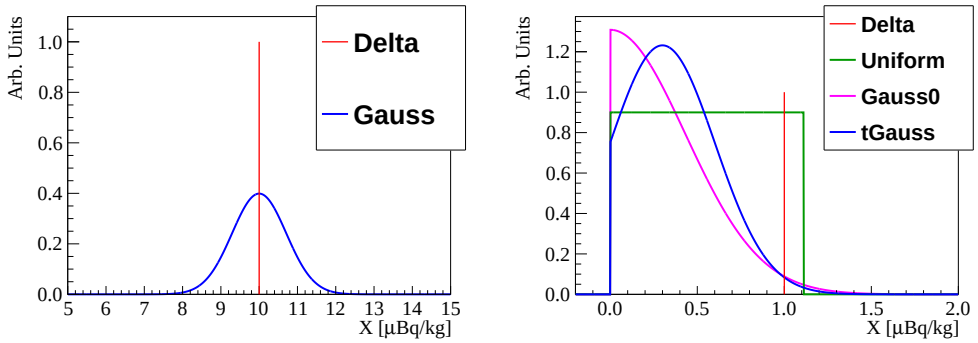
where N_{Xe} is the number of ^{136}Xe nuclei in the fiducial volume, and S_R is the mean of the upper limits saved to the array. The above described procedure corresponds to the leftmost flow from top to bottom in the diagram in Figure

[2] The sensitivity projection code is available at: `https://github.com/pnnl/sensitivity`

1. Notice that S is a fixed number despite the use of Monte Carlo method in its calculation.

4.2.2. Sensitivity based on radioassay measurements

Impurity concentrations measured in material assays are often reported in two different forms, either as a central value with an error ($\mu_i \pm \sigma_i$) or as an upper limit (ℓ_i). The following details several common ways to use them in a sensitivity calculation, as illustrated in Figure 2.



(a) Central value: $X = (10 \pm 1)$ μBq/kg (b) Limit: $X < 1$ μBq/kg (or $X = (0.30 \pm 0.43)$ μBq/kg)

Figure 2: Illustrations of prior choices considered. (Colors online)

Handling of central values. We consider two possible choices. Both of which can be expressed in terms of drawing a "true" [3]impurity concentration from a prior.

[3] *True* (in italics) represents the fixed but unknown value of a parameter in frequentist interpretation, whereas "true" (in quotes) represents a possible value of a parameter drawn from a Bayesian prior.

1. **Dirac delta prior:** $\delta(x-\mu_i)$ When the central value is large compared to the error, it is often used directly for the impurity concentrations in the sensitivity calculation, as if we have perfect knowledge.
2. **Gaussian prior:** $G(x;\mu_i,\sigma_i)$ However, when the central value is comparable to the measurement uncertainty ("just a few sigmas away from zero" for example), the knowledge of the precision of the impurity concentration may be captured with a prior describing the assay result. The "true" impurity concentration (X_i^a) is then drawn from such a prior. Arguably the most intuitive choice is a Gaussian with μ equals the central value and σ equals the measurement uncertainty ($G(\mu_i,\sigma_i)$). Note that this prior choice is also motivated by Bayesian arguments (as described in Appendix C.)

Handling of upper limits. When an upper limit is reported, we do not know the most likely value of the impurity concentration. Below are some possible ways to cope with this situation using assumed priors to once again capture the (now more limited) knowledge gained from the radioassay measurement.

1. **Dirac delta prior** $\delta(x-\ell_i)$. The upper limit is used for the "true" impurity concentration. As one might expect, the calculated sensitivity could be worse (or more "conservative") than the actual *true* sensitivity, as we will show in Section 6. Also, this method does not respect the confidence level of the reported upper limit, if it is associated with one.
2. **Uniform prior** $U_{(0,\ell_i/0.9)}(x)$. Another approach is to assume no further knowledge than is given by the upper limit itself. In other words, the "true" impurity concentration is considered equally likely to lie anywhere between 0 and the reported upper limit. As a technical detail,

the uniform prior is defined to extend beyond the reported upper limit to preserve the confidence level of 90%.

3. **Gaussian prior** A Gaussian prior seems a natural choice to represent the "true" impurity concentration, but the challenge here is to set both parameters μ and σ when only one value (the upper limit ℓ_i) is available. We consider two possible strategies:

   (a) **Half-Gaussian prior centered at zero (Gauss0)** $G(x; 0, \ell_i/1.64)$ The reporting of an upper limit implies that the actual *true* impurity concentration could be zero. One could posit that the most likely value is indeed zero and the non-observation of impurities is evidence for such a state of affairs. To express this belief, a prior would thus be formed with a half-Gaussian with μ equals 0 and σ adjusted so that the tail area conforms with the confidence level of the reported limit (i.e. $\int_{\ell_i}^{\infty} G(x; 0, \sigma)\ dx = 0.1$, if the C.L. is assumed to be 90%).

   (b) **Truncated Gaussian (tGauss)** $G(x; \mu_i, \sigma_i)$ If we have access to the measurement counts that beget the limit, there is another option motivated by Bayesian arguments (as elaborated in Appendix C.) If we set μ to be $\frac{1}{D} \cdot (s - b)$ (as in Equation 3) which may be negative, and set σ to the usual measurement uncertainty, we can then form a Gaussian. This Gaussian will be truncated at zero to remove unphysical impurity concentrations. However, this is not always feasible as this requires μ_i and σ_i while usually only ℓ_i is reported. This last point will be discussed further in Section 6.

5. Projected sensitivity under different scenarios

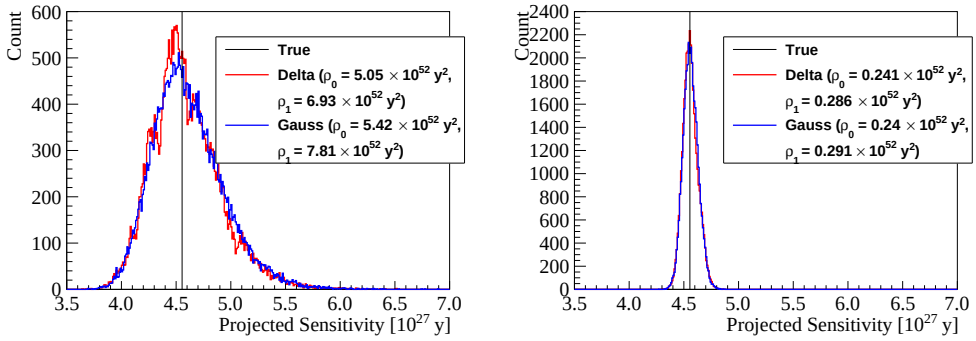
5.1. Detector with identical parts

First consider a detector consisting of N identical parts, each part having a hit efficiency of $\varepsilon = 3.171 \times 10^{-4}/N$ so that the *true* total background rate is 1 count per year when $X = 100$ μBq/kg. Recall that $X = 100$ μBq/kg is well above the detection limit of our HPGe assay detector ($\sim$23.8 μBq/kg.)

When $X = 100$ μBq/kg, only the prior choice for central values is relevant as the probability of reporting an upper limit is vanishingly small. Figure 3 compares the projected sensitivities for using the Dirac delta prior and the Gaussian prior in such a case, for $N = 1$ and $N = 20$. As seen in the figures, the difference between the two priors is relatively small (as compared to the results that follow). For ease of comparison, in all following calculations, the Dirac delta prior is always used if a central value is reported by the HPGe assay instrument.

When the impurity concentrations are close to or even below the detection limit of the HPGe assay detector, the prior choices for upper limits become more relevant as upper limits are now reported more often. Figures 4 and 5 show the projected sensitivities for this detector with impurity concentrations X lower than 100 μBq/kg. The distributions for different priors are seen to show some distinctive shapes as X becomes smaller.

As seen in the figures, the sensitivity calculated using the Dirac delta prior begins to visibly diverge from the *true* sensitivity when $X = 40$ μBq/kg, while the other priors only begin to do so at $X = 30$ μBq/kg. At $X = 10$ μBq/kg, all distributions deviate substantially from the *true* value and they underestimate more often than overestimate.



(a) N = 1 (b) N = 20

Figure 3: Comparison between the Dirac delta prior and the Gaussian prior for assay measurements reporting central values and errors, assuming detector with N identical parts, each part having impurity concentration X = 100 μBq/kg, and $\varepsilon = 3.171 \times 10^{-4}/N$. The reduction in spread for large N can be attributed to the independence of the assays performed for the N parts. Each histogram contains 35000 realizations of assay campaigns. The risks ρ_0 and ρ_1 are defined in Section 6. (Colors online)

We checked that when the hit efficiency is doubled to $\varepsilon = 6.342 \times 10^{-4}/N$, almost identical features are seen at the same X values. (This means that the *true* total background rate is 2 counts per year when $X = 100$ μBq/kg.) This is expected as the shapes of the distributions of the projected sensitivities should only depend on the assay measurements and the way they are interpreted as priors, but not on the total background rate.

5.2. Realistic detectors

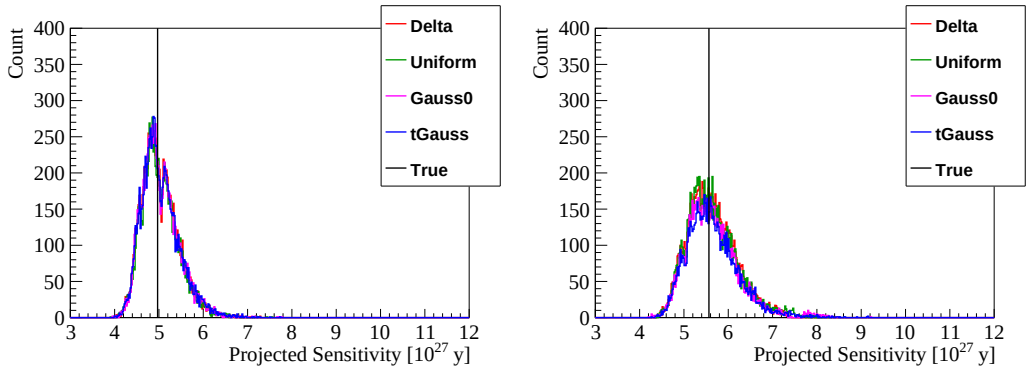
So far, we have only considered detectors with identical parts, which contribute equally to the total background. As we have observed in general, in an actual detector, the background contributions by parts often loosely follow an exponential distribution (e.g. [4, 6]) and so will we stipulate for this analysis.

Let us consider a detector that has 10 parts (N=10) and that the background contribution by the ith part (R_i) is proportional to $e^{-\frac{i-1}{2}}$. In other words, part 1 contributes most to the total background and part 10 the least, and their contributions differ by about a factor of 100.

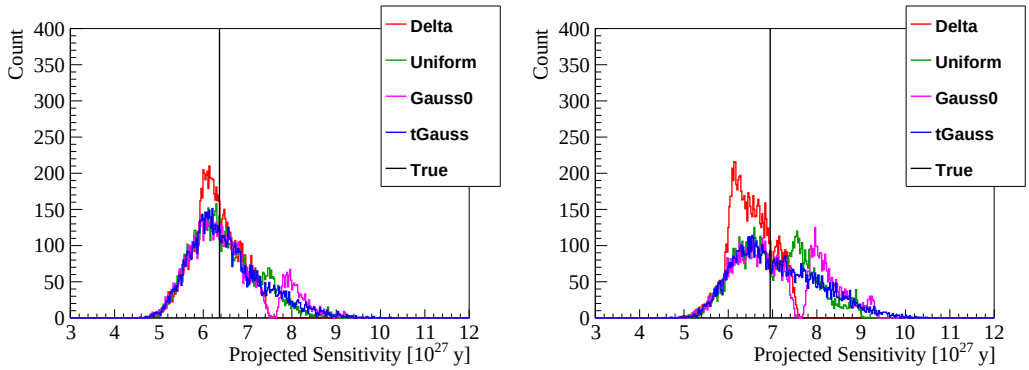
Let us consider three scenarios for the impurity concentrations of each part,

- Scenario 1: X_i increases linearly with i: $X_i = X_0 i$.
- Scenario 2: X_i remains constant: $X_i = X_0 \frac{N+1}{2}$.
- Scenario 3: X_i decreases linearly with i:
  $X_i = X_0(N + 1 - i)$.

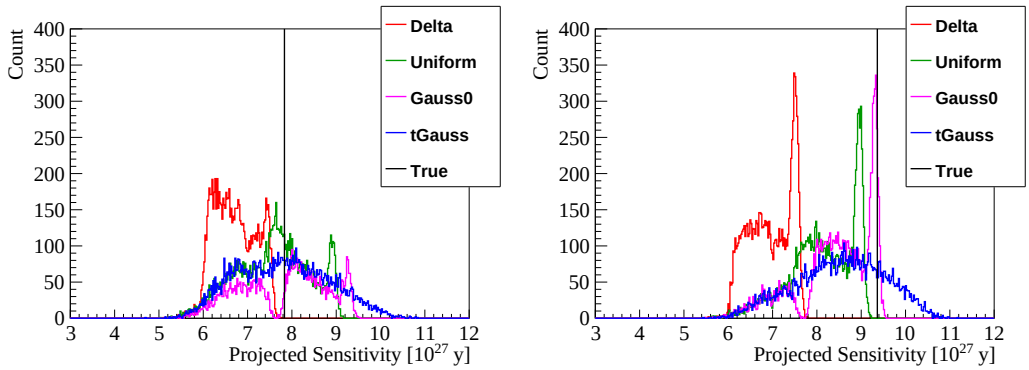
By fixing the total background rate $\sum R_i$, the hit efficiencies for each part can be defined.



(a) $X = 80$ μBq/kg (b) $X = 60$ μBq/kg

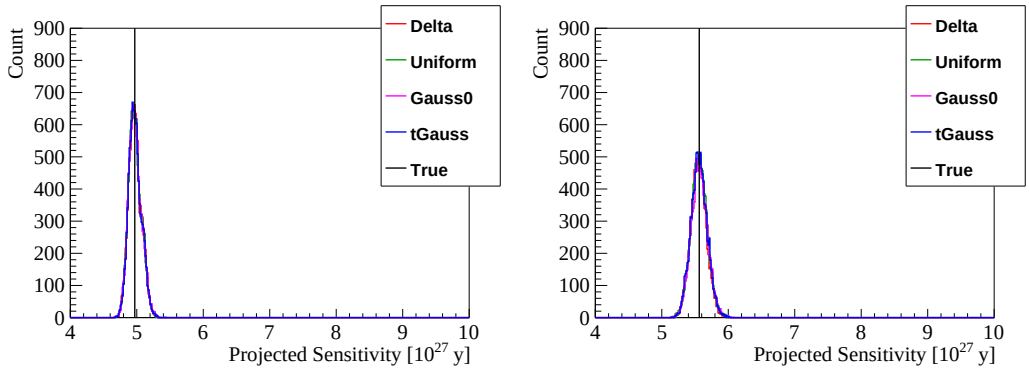


(c) $X = 40$ μBq/kg (d) $X = 30$ μBq/kg

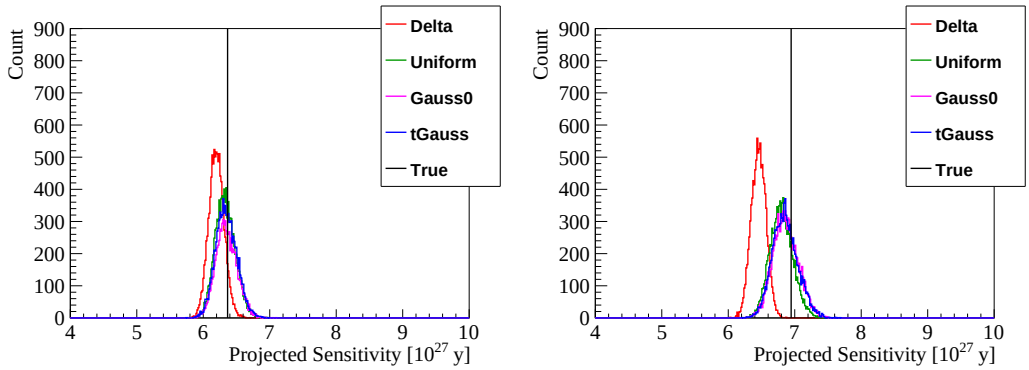


(e) $X = 20$ μBq/kg (f) $X = 10$ μBq/kg

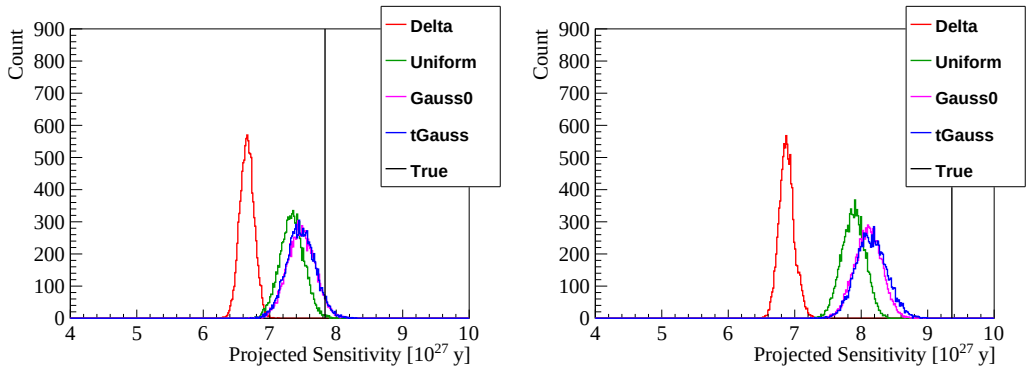
Figure 4: Projected sensitivities for different priors and different impurity concentrations X, for $N = 1$ and $\varepsilon = 3.171 \times 10^{-4}$. Notice that panel (a) having $X = 80$ μBq/kg is very similar to Figure 3a where $X = 100$ μBq/kg. As the impurity concentration decreases toward $X = 10$ μBq/kg (panel (f)), three of the four choices of prior show similar but highly-asymmetric distribution shapes. (Colors online)



(a) $X = 80$ μBq/kg (b) $X = 60$ μBq/kg

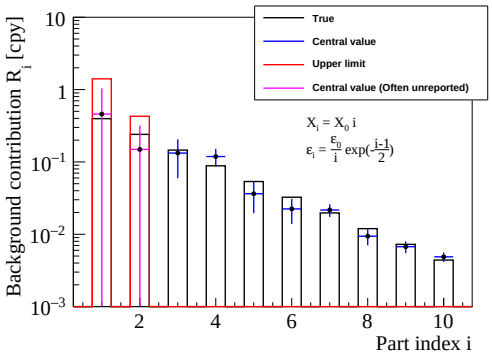


(c) $X = 40$ μBq/kg (d) $X = 30$ μBq/kg

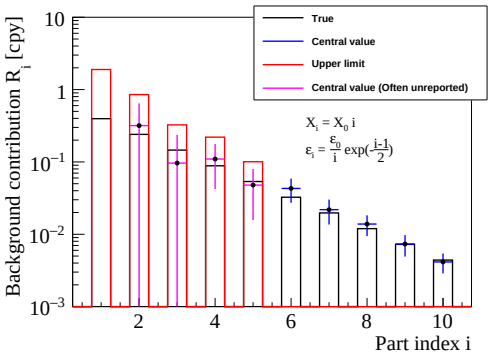


(e) $X = 20$ μBq/kg (f) $X = 10$ μBq/kg

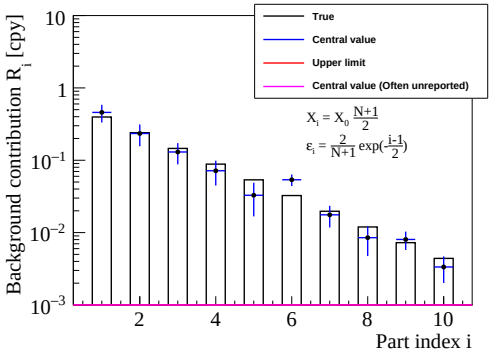
Figure 5: Projected sensitivities for different priors and different impurity concentrations X, for $N = 20$ and $\varepsilon = 1.585 \times 10^{-5}$. Here, the distributions are visibly closer to a Gaussian shape due to the independence of the assay measurements of the parts. (Colors online)



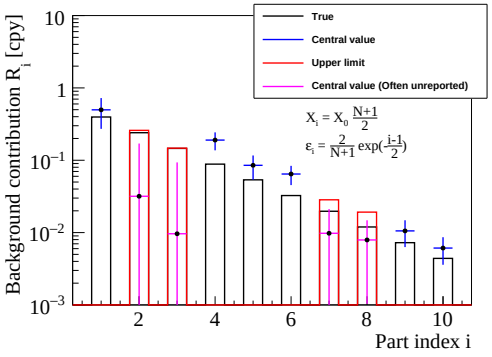
(a) $X_0 = 10$ μBq/kg, $X_i = X_0 i$



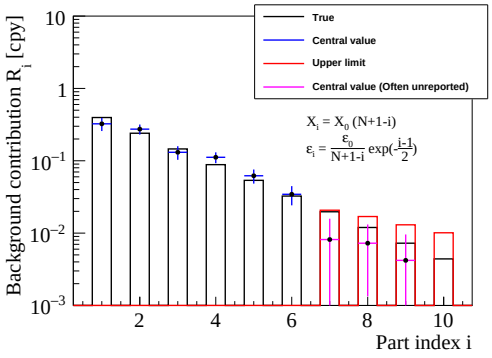
(d) $X_0 = 5$ μBq/kg, $X_i = X_0 i$



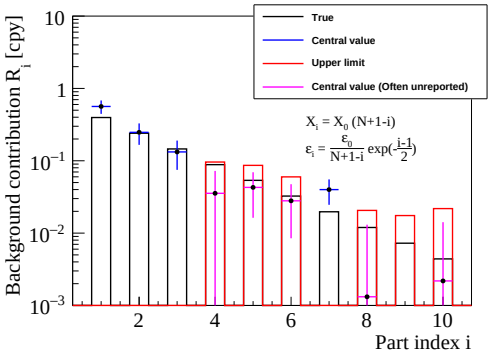
(b) $X_0 = 10$ μBq/kg, $X_i = X_0 \frac{N+1}{2} = 55$ μBq/kg



(e) $X_0 = 5$ μBq/kg, $X_i = X_0 \frac{N+1}{2} = 27.5$ μBq/kg

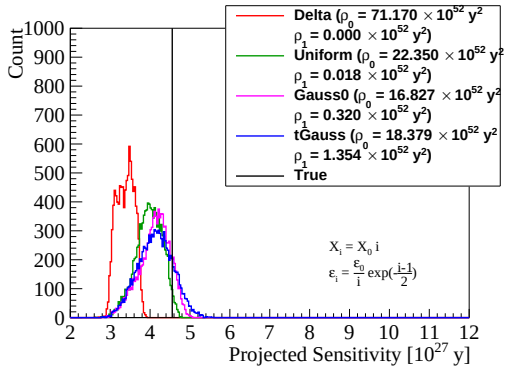


(c) $X_0 = 10$ μBq/kg, $X_i = X_0(N+1-i)$

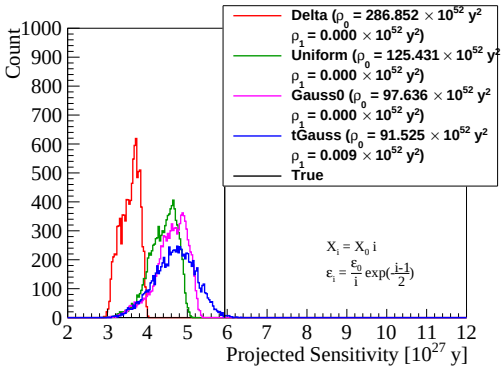


(f) $X_0 = 5$ μBq/kg, $X_i = X_0(N+1-i)$

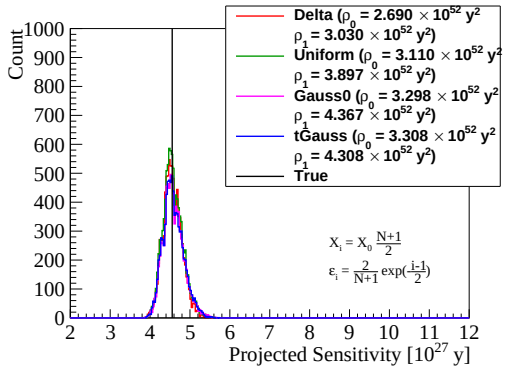
Figure 6: The black bars show the background contributions by each part assuming the realistic scenarios described in Section 5.2. The colored data points and bars represent the expected background contribution based on the results of one realization of an assay campaign: shown in blue are central values and errors, red upper limits, and magenta the underlying central values and errors when an upper limit should be reported. The distributions of projected sensitivities calculated from ensembles of assay campaign realizations such as this one are shown in Figure 7. ($N = 10$, $\varepsilon_0 = 1.256 \times 10^{-3}$) (Colors online)



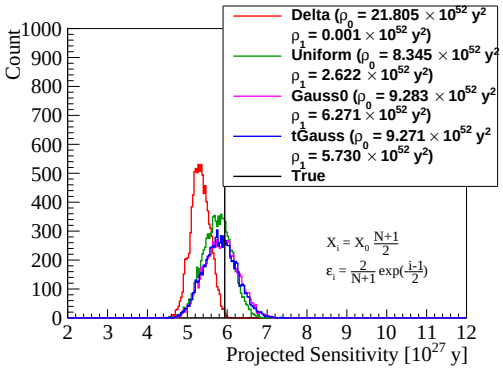
(a) $X_0 = 10$ μBq/kg, $X_i = X_0 i$



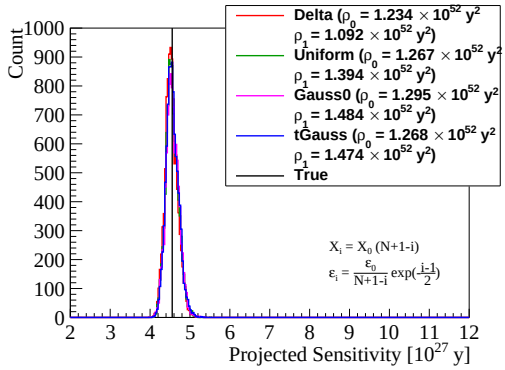
(d) $X_0 = 5$ μBq/kg, $X_i = X_0 i$



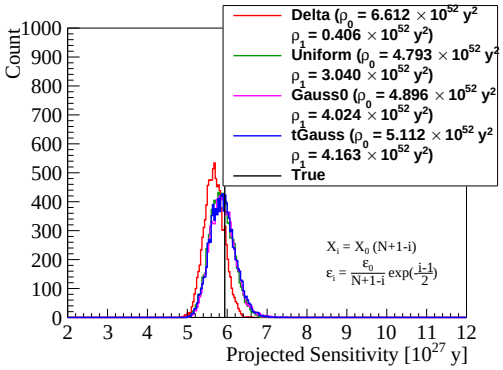
(b) $X_0 = 10$ μBq/kg, $X_i = X_0\frac{N+1}{2} = 55$ μBq/kg



(e) $X_0 = 5$ μBq/kg, $X_i = X_0\frac{N+1}{2} = 27.5$ μBq/kg



(c) $X_0 = 10$ μBq/kg, $X_i = X_0(N+1-i)$



(f) $X_0 = 5$ μBq/kg, $X_i = X_0(N+1-i)$

Figure 7: Projected sensitivities for the realistic scenarios described in Section 5.2. Each data point in the histograms is calculated using the assay results from a realization of an assay campaign such as the one shown in Figure 6. ($N = 10$, $\varepsilon_0 = 1.256 \times 10^{-3}$) (Colors online)

Figures 6a, 6b, and 6c illustrate the three scenarios when X_0 is set to 10 μBq/kg, and Figures 6d, 6e, and 6f show similar plots for $X_0 = 5$ μBq/kg. Figure 7 shows the distributions of the projection sensitivities for the above scenarios.

With a configuration such as Scenario 1, the sensitivity estimation is susceptible to the prior choice for upper limits, as the background contribution from the largest contributor is more likely derived from an upper limit. Whereas in Scenario 3, prior choice for central values plays a more important role in sensitivity estimation.

6. Discussion

In the previous section, we presented the raw results of calculating projected sensitivities under different experimental scenarios and choices of priors used to interpret assay results. Now we proceed to evaluate these results.

6.1. Quantifying conservativeness

One of the factors in evaluating a choice of assay result prior is the perceived *conservativeness* of the resulting projected sensitivity. Necessarily then, it is important to quantify *conservativeness* in order to guide our choice. To our knowledge this step of quantifying a notion of conservativeness has not been considered in the literature of low background physics experiments. We could consider projected sensitivity as an estimator of the *true* sensitivity where the prior choice can be seen as a parameter for this estimator. Choosing a different prior for assay results will generate a different estimator. To evaluate the goodness of an estimator, the quadratic loss function (QLF) is often used. However, being symmetric, QLF is inadequate in our situation

because, in the case of limit-setting experiments, we may disfavor an overestimate more than an underestimate while QLF cannot reflect that. To allow assigning different losses to underestimates and overestimates, we can define an asymmetric loss function as follows,

$$L_\alpha(X, \hat{S}_p(Y)) = \begin{cases} \frac{1+\alpha}{2}[\hat{S}_p(Y) - S(X)]^2 & \text{if } \hat{S} > S \\ \frac{1-\alpha}{2}[\hat{S}_p(Y) - S(X)]^2 & \text{if } \hat{S} \leq S \end{cases} \tag{11}$$

where X denotes the set of *true* impurity concentrations of all parts $\{X_i\}$ and Y denotes the set of assay results $\{Y_i\}$ where $Y_i = \mu_i \pm \sigma_I$ or ℓ_i. $\hat{S}_p = \hat{S}_p(Y)$ is the projected sensitivity calculated from assay results Y using the prior choice p. We propose to use α as a measure of conservativeness in this study. A positive α represents more disfavor for overestimates than underestimates, a negative α has the opposite effect, and $\alpha = 0$ is effectively the ordinary QLF which treats underestimates and overestimates equally. Figure 8 shows some example loss functions at different α's.

An estimator is optimal if it minimizes the expected value of loss as a function of the *true* impurity concentrations X, also known as *risk*, which is defined as,

$$\rho_\alpha(X, \hat{S}_p) = \int L_\alpha(X, \hat{S}_p(Y)) \prod_i A_{X_i}(Y_i) dY_i \tag{12}$$

where $A_{X_i}(Y_i)$ is the probability distribution of Y_i reported by an assay measurement given the *true* impurity concentration X_i. (Notice that ρ_0 is the usual mean squared error.) We will use *risk* (ρ_α) defined above as the figure of merit to compare different prior choices.

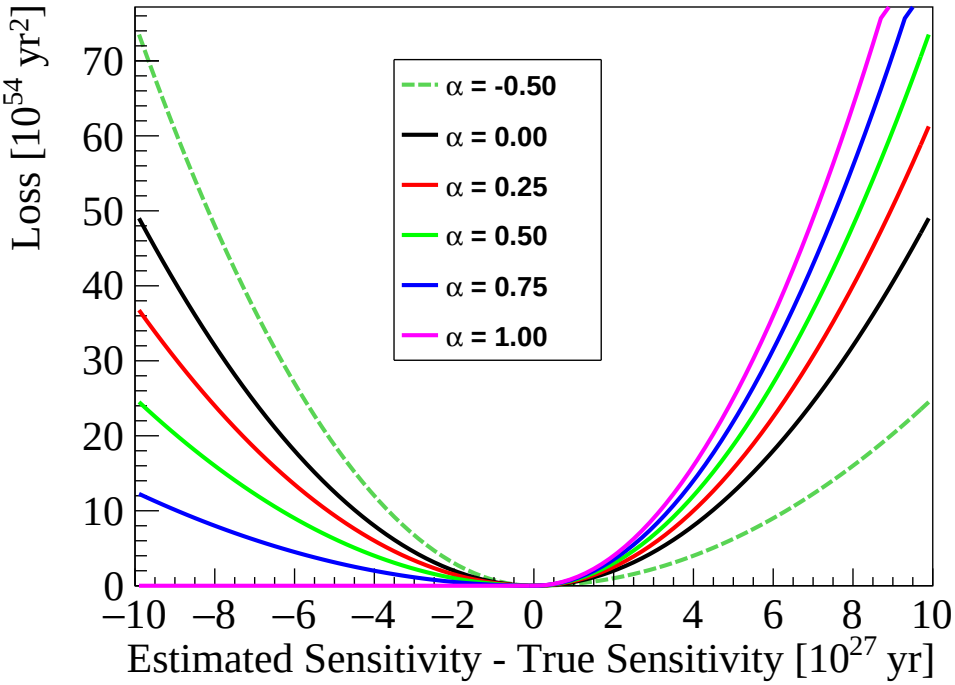


Figure 8: Examples of the loss function defined in Equation 11 with different values of α. In this paper, only positive values of α are considered. (Colors online)

6.1.1. Prior choice for central values

If we take the risks for the Dirac delta prior and the Gaussian prior at face value (as shown in the legends in Figure 3), the Dirac delta prior seems to be the preferred choice whether α is 0 or 1. In fact, since ρ_α depends linearly on α, we can deduce that, $\rho_\alpha(X, \hat{S}_D) < \rho_\alpha(X, \hat{S}_G)$ for all $\alpha \in [0, 1]$. Therefore, the Dirac delta prior is preferred regardless of your choice of $\alpha \in [0, 1]$. However, the advantage diminishes as N increases.

As compared to the differences due to the prior choice for upper limits, the difference between the two priors for central values appears small. Therefore, the Dirac delta prior is preferred but not strongly.

6.1.2. Prior choice for upper limits

As indicated in Figure 7, the best prior choice for upper limits, as suggested by the figure-of-merit ρ_α, appears to depend on the preferred value of α. For those who prefer $\alpha = 1$ (most conservative), the Dirac delta prior is clearly the best choice among the four priors considered. For $\alpha = 0$, the situation is more complex. For the two cases where central values are more often reported (Figures 7b and 7c), the Dirac delta prior is the best choice. For the four other cases where upper limits are more often reported, there is no clear best choice among the Uniform, the Gaussian-at-zero, and the Truncated Gaussian priors. It seems to depend on the particular distribution of impurity concentrations, though these three priors are clearly better than the Dirac delta prior in these four cases.

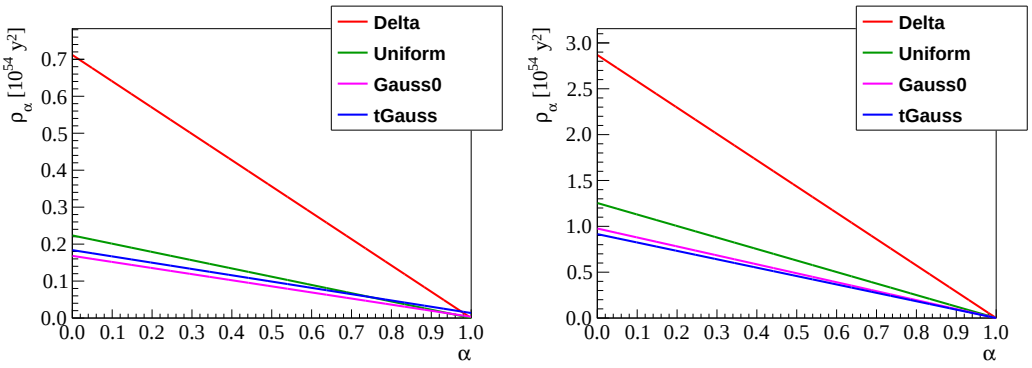
6.2. Appropriate values of α

As shown in the results above, risk depends on the value of α. Now, a question remains: How to assign a value to α that reflects our relative disfavor for underestimates and overestimates? Here are some considerations:

- α is a subjectively-chosen "hidden" variable which manifests itself only through the choice of a prior. Therefore, values of α that result in the same prior choice can be considered identical for the purpose of this study.

- In Scenario 1 considered above where upper limits dominate, the Dirac delta prior is *better* than the other priors only when α is very close to 1 ($>\sim$0.98, see Figures 9a and 9b). For other values of α, the Truncated Gaussian prior, the Gaussian-at-zero prior, and the Uniform prior all give similar risk values, indicating that they are almost equally *good* when judged by this metric.

In practice, some collaborations effectively choose the Dirac delta prior for upper limits (See Table 2). This reflects their implicit choice of an α that is possibly very close to 1. Essentially this choice uses positively biased assay results in sensitivity calculations, to result in a negatively biased projected sensitivity, apparently being "conservative" in reporting a projected sensitivity. Initially, this appears to be a prudent choice. However, as seen in the projected sensitivity distributions shown previously in this paper, overestimations cannot be avoided no matter which prior is chosen. Moreover, taking the upper limits verbatim poses another problem. The upper limits may be reported at any confidence levels (say, 90%, 95% or 3σ), depending on



(a) $X_0 = 10$ μBq/kg, $X_i = X_0 i$ (b) $X_0 = 5$ μBq/kg, $X_i = X_0 i$

Figure 9: Risk as a function of α for Scenario 1 considered in Section 5.2. Low risk (vertical axis) may be considered subjectively "better". (Colors online)

Collaboration	Central values and errors	Upper limits	Ref.
Majorana Demonstrator	Delta	Delta	[1]
NEXT	Delta	Delta	[2]
PandaX III	Delta	Delta	[3]
CUORE	Gaussian	*(included as systematics)*	[4]
CUORE-0	Gaussian	Half Gaussian at zero	[5]
nEXO	Gaussian	Half Gaussian at zero	[6]

Table 2: Priors chosen by some experiment collaborations for their sensitivity projections.

the common practice of the particular assay technique and/or assay facility. They result in different amounts of negative bias in the projected sensitivities. However, there is no *a priori* reason why a negative bias of a certain magnitude should be introduced, other than simply convenience ("just use the upper limit as reported"). Thus, the projected sensitivity calculated is contingent on the choice of confidence level by the assayer, but not entirely on the radioimpurity concentrations of the samples and the assay sensitivities.

To remove this subjectivity, the response would be to aim for an unbiased estimate of the sensitivity (i.e. $\alpha = 0$). The Truncated Gaussian prior is arguably the best choice because in addition to its low risk value at $\alpha = 0$, it is also motivated by Bayesian considerations on the assay measurements (as discussed in Appendix C.) Since forming the Truncated Gaussian prior requires information that is sometimes unavailable (e.g. μ and σ when only the upper limit is reported), in those cases, both the Gaussian-at-zero prior and the Uniform prior are viable alternatives.

6.3. Estimating the spread of projected sensitivity, σ_S

The remaining concern for overestimation can be mitigated by quantifying the spread (σ_S) of the projected sensitivity due to statistical uncertainty in the assay results.

To estimate σ_S, we can treat the assay results as Gaussian-distributed nuisance parameters, and propagate the uncertainties using a Monte Carlo method. This is sometimes known as the "pull" method (described, for example, in [15].) The quantity σ_S can then be seen as the standard deviation of the resulting projected sensitivity distribution.

We could check to see if σ_S represents the correct coverage probabilities for the above realistic scenarios using a z-score defined as,

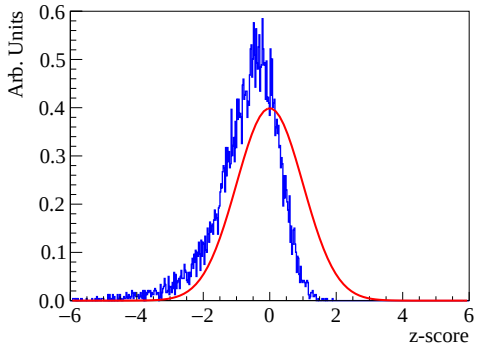
$$z = \frac{\hat{S} - S}{\sigma_S} \tag{13}$$

where $\hat{S}$ and S are respectively the projected sensitivity (calculated using the Truncated Gaussian prior) and the *true* sensitivity. We can then compare the distribution of z with the standard Gaussian distribution.

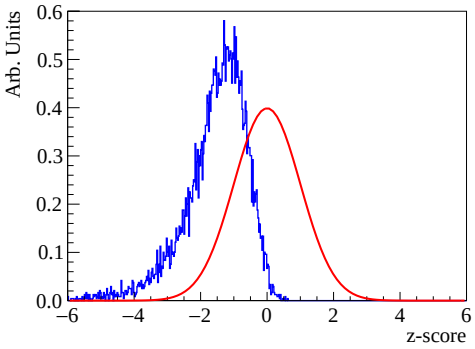
Shown in Figure 10 are the distributions of the z-scores of 10000 instances of assay campaigns for the three realistic scenarios with X_0 set to 10 μBq/kg and 5 μBq/kg, and Table 3 shows their 1-, 2- and 3-σ coverage probabilities. When the total background is dominated by parts with high X (Scenarios 2 and 3), the deviations of the z distributions from Gaussian are small, and the coverage probabilities are close to what is expected of a Gaussian distribution. In Scenario 1 where low-X parts dominate, we see a significant deviation from the Gaussian. This is expected since our sensitivity projection method generally underestimates sensitivity in such cases as seen in Figures 7a and 7d, while σ_S only quantifies the statistical uncertainty arising from assay measurements. The amount of deviation can be reduced by improving assay techniques.

7. Conclusion

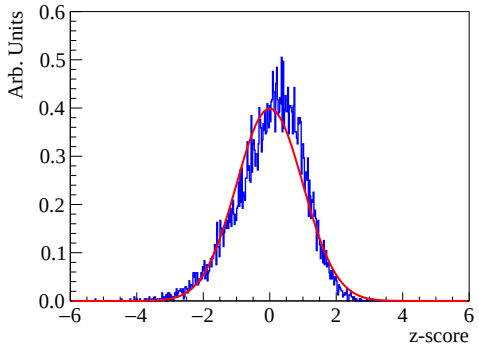
We have created a model of the sensitivity projection for a hypothetical $0\nu\beta\beta$ experiment, starting from the assay of detector materials, up to the calculation of the projected sensitivity.



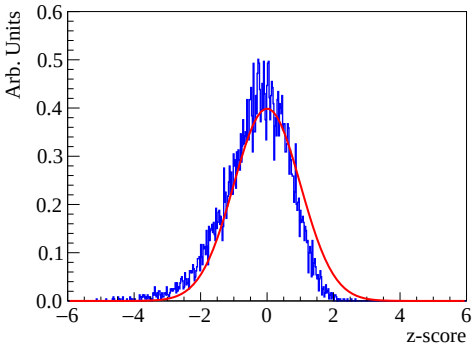
(a) $X_0 = 10$ μBq/kg, $X_i = X_0 i$



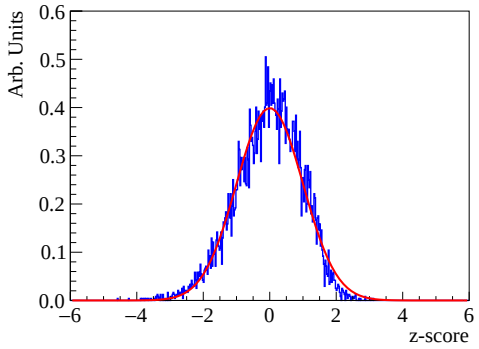
(d) $X_0 = 5$ μBq/kg, $X_i = X_0 i$



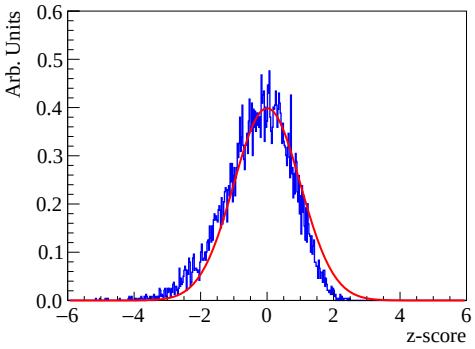
(b) $X_0 = 10$ μBq/kg, $X_i = X_0 \frac{N+1}{2} = 55$ μBq/kg



(e) $X_0 = 5$ μBq/kg, $X_i = X_0 \frac{N+1}{2} = 27.5$ μBq/kg



(c) $X_0 = 10$ μBq/kg, $X_i = X_0(N+1-i)$



(f) $X_0 = 5$ μBq/kg, $X_i = X_0(N+1-i)$

Figure 10: Distributions of z-scores for the realistic scenarios considered in Section 5.2 are plotted in blue and the standard Gaussian ($\mu = 0, \sigma = 1$) is drawn in red for comparison. (Colors online)

	$X_0 = 10$			$X_0 = 5$			
σ	Scenario 1	Scenario 2	Scenario 3	Scenario 1	Scenario 2	Scenario 3	Gaussian
1	0.685	0.692	0.693	0.303	0.708	0.684	0.683
2	0.914	0.958	0.962	0.746	0.945	0.944	0.955
3	0.975	0.995	0.997	0.922	0.989	0.992	0.997

Table 3: Coverage probabilities for the three realistic scenarios with $X_0 = 10$ and 5, considered in Section 5.2.

Using this model, we evaluated how the different interpretations of assay results as priors in the sensitivity projection procedure affects the projected sensitivity value. We evaluated the results using the notion of "conservativeness", which is understood as our subjective aversion to overestimating the sensitivity. This can be quantified by the parameter $\alpha \in [-1, 1]$ of an asymmetric loss fuction modified from the usual QLF. Based on the loss function, for each prior, we can define risk ρ, which is used as the figure of merit for comparing the priors.

Based on the figure of merit ρ_0, we have shown that when assay results produce central values and errors well above the sensitivity of the assay technique, the Dirac delta prior is recommended, though its advantage over the Gaussian prior is minimal. In the case that the impurity concentrations are below the sensitivity of the assay technique and upper limits are reported, the Truncated Gaussian, Gaussian-at-zero, and Uniform priors all give similar results. The Truncated Gaussian prior has the advantage that it can be motivated by Bayesian arguments, although it requires additional informa-

tion to be reported by the assayers. The Dirac delta prior for upper limits is shown to have the worst figure of merit under all but the most "conservative" assumptions (e.g. $\alpha > 0.98$ in Scenario 1 considered above.)

To ease the concern for overestimation, we also suggested calculating σ_S which estimates the error in S stemming from statistical fluctuations in the assay process. Experiments may report "$S \pm \sigma_S$" as their projected sensitivity, explicitly stating the uncertainty due to assay measurements.

Appendix A. HPGe sensitivity

Let X be the impurity concentration of a sample, assayed by a HPGe detector with a detection sensitivity of D, and a background rate of B, for a livetime of t.

The measured sample counts and background counts, c_s and c_b, thus follow the distributions:

$$\begin{cases} c_s \sim Po(\lambda = DXt + Bt) \\ c_b \sim Po(\lambda = Bt) \end{cases} \tag{A.1}$$

where $Po(\lambda = \cdot)$ represents the Poisson distribution with mean λ.

X can be estimated by $\hat{X}$ which is defined by,

$$\hat{X} = \frac{1}{Dt}(c_s - c_b) \tag{A.2}$$

and its uncertainty is,

$$\hat{\sigma} = \frac{1}{Dt}\sqrt{c_s + c_b} \tag{A.3}$$

On average, to observe a signal, we require $\mathbb{E}(\hat{X}) > n\mathbb{E}(\hat{\sigma})$, where n is the "number of sigmas" required for declaring a detection. This is satisfied when,

$$X > \frac{n^2}{2Dt}(1 + \sqrt{1 + \frac{8Bt}{n^2}}) \tag{A.4}$$

Now, apply the above inequality to the case described in the main text. For $n = 1.64$ (i.e. 90% C.L.), $D = 1$ cps/(Bq/kg), $B = 10$ cpd, and $t = 14$ d, $X > 23.8$ μBq/kg.

Appendix B. Mean vs median upper limit as sensitivity

One could consider whether to use the *mean* or the *median* to calculate an average upper limit. If the median is used, the sensitivity as a function of background rate would exhibit a sawtooth pattern (as shown in Figure B.11). This behavior has frequently been observed, but this is counter-intuitive as it implies that a better sensitivity could be achieved by increasing the background rate by a small amount just short of reaching the next jump. However, if the mean is used, the curve becomes monotonous as one would intuitively expect. Therefore, in this study, mean sensitivity is used.

Appendix C. Motivating the Truncated Gaussian prior using Bayesian arguments

First, let's clarify the terminology. As general terminology in Bayesian statistics, the (assumed) distribution of a parameter before a measurement is called a *prior* distribution, while the distribution of the parameter after incorporating the measurement result is called a *posterior* distribution. In

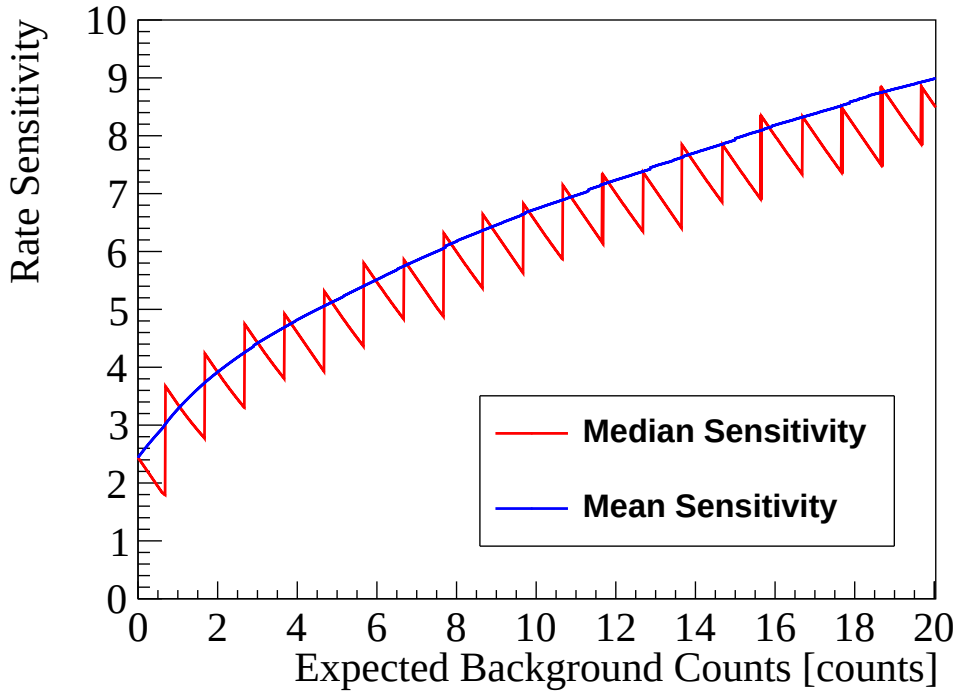


Figure B.11: Comparison between using the mean vs the median of upper limits as the sensitivity. (Colors online)

sensitivity projections, there are two stages of measurements: the first stage is the assay measurements and the second stage is the actual experiment that attempts to detect a rare physical process. The priors described in the main text are called as such since they are priors relative to the actual experiment. Though, at the same time, they are *posteriors* relative to the assay measurements. (To avoid confusion, when mentioned in this appendix, the priors in the main text are in quotes from now on.) In other words, the "priors" can, in fact, be derived using Bayes' theorem by assuming prior distributions for the impurity concentration X and the HPGe background rate B. Using the same parameter definitions as in Appendix A, the posterior distribution for X and B given c_s and c_b can be written as follows by applying Bayes' theorem,

$$\begin{aligned} P(X, B|c_s, c_b) &= AP(c_s, c_b|X, B)P(X, B) \\ &= AP(c_s|X, B)P(c_b|B)P(X)P(B) \\ &= A\frac{\lambda_s^{c_s}e^{-\lambda_s}}{c_s!}\frac{\lambda_b^{c_b}e^{-\lambda_b}}{c_b!}P(X)P(B) \end{aligned} \tag{C.1}$$

where $A = \frac{1}{P(c_s)P(c_b)}$, $\lambda_s = DXt + Bt$, and $\lambda_b = Bt$.

Now, assume the priors $P(B)$ and $P(X)$ are (improper) uniform distributions defined in $[0, \infty)$. Then, marginalizing over B, which is a nuisance parameter, gives,

$$\begin{aligned} P(X|c_s, c_b) &= \int_0^\infty P(X, B|c_s, c_b)dB \\ &= Ae^{-x}x^{c_s+c_b+1}U(c_b + 1, c_s + c_b + 2, 2x) \end{aligned} \tag{C.2}$$

where $x = DXt$, and $U(\cdot, \cdot, \cdot)$ is the confluent hypergeometric function of the second kind. We can then compare $P(X|c_s, c_b)$ with the corresponding

Truncated Gaussian "priors" for the same c_s and c_b. As shown in Figure C.12, $P(X|c_s, c_b)$ and its corresponding Truncated Gaussian "prior" are very similar in shape. Therefore, the Truncated Gaussian "prior" can be seen as an approximation to $P(X|c_s, c_b)$ which has a more complex functional form.

Another feature of $P(X|c_s, c_b)$ (and its Truncated Gaussian approximation) that other "priors" lack is that the transition between the upper limit and the central value regions is smooth. This means that the choice of C.L. by the assayer to report an upper limit has no effect on the "prior" shape, as the upper limit is not directly used in the definition of the "prior".

Acknowledgements

This work was supported by the Nuclear-physics, Particle-physics, Astrophysics, and Cosmology (NPAC) Initiative, a Laboratory Directed Research and Development (LDRD) effort at Pacific Northwest National Laboratory (PNNL). PNNL is operated by Battelle for the U.S. Department of Energy (DOE) under Contract No. DE-AC05-76RL01830.

This research was done using resources provided by the Open Science Grid (OSG), which is supported by the National Science Foundation and the U.S. Department of Energy's Office of Science.

R.H.M.T. would like to thank the organizers of the OSG User School 2017 in Madison, Wisconsin, for their hospitality and for offering the opportunity to learn and use the OSG. The authors would also like to thank Ben Loer, Kevin Anderson, Paul Eslinger, Scott Cooley, and Jan Strube for their valuable feedback and suggestions.

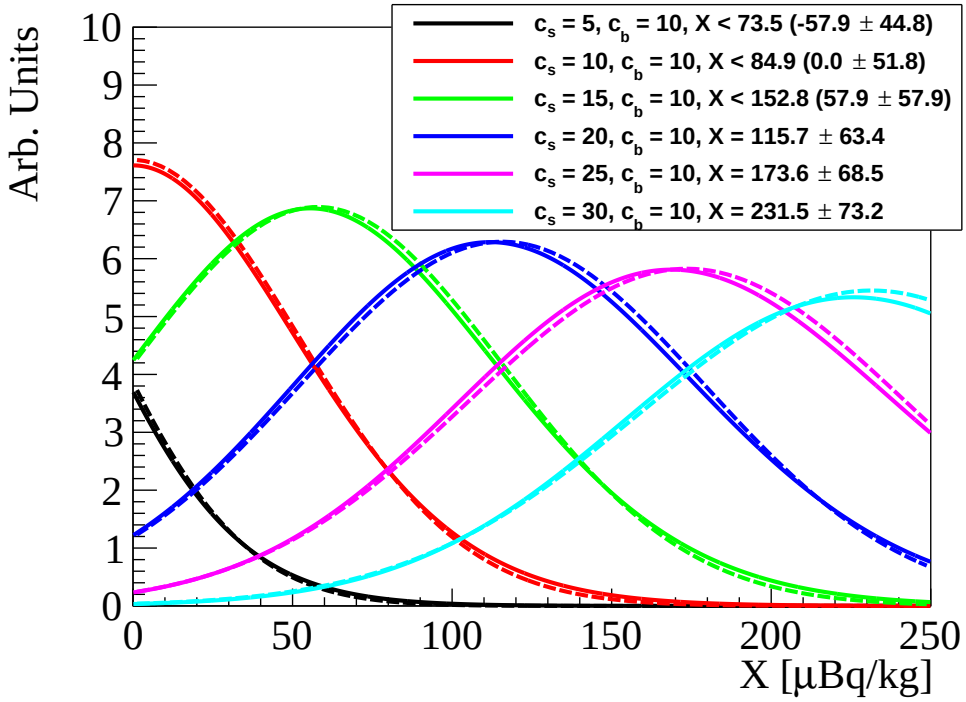


Figure C.12: Comparison between posteriors derived using Bayes' theorem assuming uniform priors for X and B (solid lines) and Truncated Gaussian "priors" (dashed lines) for some values of c_s and c_b. Here, $D = 1$ and $t = 1$ d. With such parameters, having $X > 102$ μBq/kg is required to observe a signal on average. (Colors online)

References

[1] N. Abgrall, et al., The Majorana Demonstrator radioassay program, Nuclear Instruments and Methods in Physics Research Section A: Accelerators, Spectrometers, Detectors and Associated Equipment 828 (2016) 22–36. doi:http://dx.doi.org/10.1016/j.nima.2016.04.070.
URL http://www.sciencedirect.com/science/article/pii/S0168900216302832

[2] S. Cebrián, et al., Radiopurity assessment of the energy readout for the NEXT double beta decay experiment, Journal of Instrumentation 12 (2017) T08003.

[3] X. Chen, et al., PandaX-III: Searching for neutrinoless double beta decay with high pressure ^{136}Xe gas time projection chambers, Sci. China Phys. Mech. Astron. 60 (2017) 061011.

[4] C. Alduino, et al., The projected background for the CUORE experiment, Eur. Phys. J. C 77 (2017) 543.

[5] C. Alduino, et al., Measurement of the two-neutrino double-beta decay half-life of ^{130}Te with the CUORE-0 experiment, Eur. Phys. J. C 77 (2017) 13.

[6] J. B. Albert, et al., Sensitivity and discovery potential of the proposed nEXO experiment to neutrinoless double-β decay, Physical Review C 97 (2018) 065503.

[7] D. Leonard, et al., Systematic study of trace radioactive impurities in candidate construction materials for EXO-200, Nuclear Instruments

and Methods in Physics Research Section A: Accelerators, Spectrometers, Detectors and Associated Equipment 591 (3) (2008) 490 – 509. doi:http://dx.doi.org/10.1016/j.nima.2008.03.001.
URL http://www.sciencedirect.com/science/article/pii/S016890020800346X

[8] E. Aprile, et al., Material screening and selection for XENON100, Astroparticle Physics 35 (2011) 43–49. doi:10.1016/j.astropartphys.2011.06.001.

[9] J. Loach, J. Cooley, G. Cox, Z. Li, K. Nguyen, A. Poon, A database for storing the results of material radiopurity measurements, Nuclear Instruments and Methods in Physics Research Section A: Accelerators, Spectrometers, Detectors and Associated Equipment 839 (2016) 6 – 11. doi:http://dx.doi.org/10.1016/j.nima.2016.09.036.
URL http://www.sciencedirect.com/science/article/pii/S0168900216309639

[10] G. J. Feldman, R. D. Cousins, A unified approach to the classical statistical analysis of small signals, Physics Review D 57 (1998) 3873–3889. doi:10.1103/PhysRevD.57.3873.

[11] B. D. LaFerriere, T. C. Maiti, I. J. Arnquist, E. W. Hoppe, A novel assay method for the trace determination of Th and U in copper and lead using inductively coupled plasma mass spectrometry, Nuclear Instruments and Methods in Physics Research Section A 775 (2015) 93–98. doi:10.1016/j.nima.2014.11.052.

[12] I. J. Arnquist, E. W. Hoppe, M. Bliss, J. W. Grate, Mass spectrometric determination of uranium and thorium in high radiopurity polymers using ultra low background electroformed copper crucibles for dry ashing, Analytical Chemistry 5 (2017) 3101–3107. doi:10.1021/acs.analchem.6b04854.

[13] G. F. Knoll, Radiation Detection and Measurement, 3rd Edition, Wiley, 2000.

[14] A. Ulianov, O. Müntener, U. Schaltegger, The ICPMS signal as a Poisson process: a review of basic concepts, Journal of Analytical Atomic Spectrometry 30 (2015) 1297.

[15] G. L. Fogli, E. Lisi, A. Marrone, D. Montanino, A. Palazzo, Getting the most from the statistical analysis of solar neutrino oscillations, Physical Review D 66 (2002) 053010.

[16] R. Pordes, et al., The Open Science Grid, Journal of Physics: Conference Series 78 (2007) 012057doi:10.1088/1742-6596/78/1/012057.

[17] I. Sfiligoi, D. C. Bradley, B. Holzman, P. Mhashilkar, S. Padhi, F. Wurthwein, The pilot way to grid resources using glideinWMS, 2009 WRI World Congress on Computer Science and Information Engineering 2 (2009) 428–432. doi:10.1109/CSIE.2009.950.